Earth Planet. Sci. Lett. 627 (2024) 118560

Contents lists available at ScienceDirect

Earth and Planetary Science Letters

journal homepage: www.elsevier.com/locate/epsl

Variable oxidizing capacity of slab-derived fluids: Insights from Fe and S speciation in glasses from the Troodos Ophiolite

L.M. Saper [*,a,b,1], M. Brounce [c], D. Woelki [d], R. Cao [a], G. Bromiley [a]

[a] School of Geosciences, Grant Institute, University of Edinburgh, Edinburgh EH9 3FE, United Kingdom
[b] Division of Geological and Planetary Sciences, California Institute of Technology, Pasadena, CA, United States
[c] Earth and Planetary Sciences, University of California Riverside, Riverside, CA, United States
[d] Institut für Geo- und Umweltnaturwissenschaften, Mineralogie und Petrologie, Albert-Ludwigs-Universität Freiburg, Freiburg im Breisgau, Germany

ARTICLE INFO

Edited by Editor: Dr L Coogan

Keywords:
Oxygen fugacity
Subduction
Metasomatism
Oxidizing capacity
XANES
Troodos

ABSTRACT

Oxygen fugacity (fO_2) varies systematically across tectonic environments. The typically high fO_2 recorded in arc settings relative to oceanic ridges is attributed to recycling of oxidized materials derived from subducting slabs into regions of the mantle that undergo partial melting. To evaluate further the relationship between fO_2 and mantle metasomatism, Fe and S X-ray Absorption Near-Edge Structure measurements were conducted on volcanic glass wafers sampled across the extrusive section of the Troodos Ophiolite, Cyprus, which is a type locality for studying the influence of subduction on mantle melting processes and the generation of oceanic crust. The glasses record fO_2 values relative to the quartz-fayalite-magnetite (FMQ) buffer of FMQ+0.13±0.16(1σ) to FMQ+0.74±0.23(1σ) upon quenching at the seafloor. At a given MgO content, the fO_2 values recorded by the Troodos glasses do not vary systematically based on type (i.e., boninitic versus tholeiitic) nor by sampling location, indicating that the lavas were derived from primary melts and mantle sources that were indistinguishable in their initial fO_2 levels. The glass fO_2 values do not vary with dissolved H_2O contents, nor with trace element ratios (e.g., Ba/La, Ce/Pb) and Pb and Sr isotopic compositions, all used to monitor interaction of slab-derived materials with the Troodos mantle source. The decoupling of fO_2 and H_2O and fluid-mobile elements renders the Troodos an important endmember for interpreting global variations in the redox state of mantle melts formed in subduction-influenced settings. For example, the Troodos glasses are reduced relative to Izu-Bonin boninites and melt inclusions from Mariana and Cascades arc volcanoes, despite overlapping and elevated H_2O contents, Ba/La, and S/Dy relative to mid-ocean ridge basalts. The lack of correlation between fO_2 and volatile contents and with proxies for subduction influence in the Troodos glasses is similar to basalts formed in back-arc environments and in near-trench settings in Izu-Bonin-Mariana. Such comparisons suggest that the slab-derived fluids that infiltrated the Troodos melting region were derived from a shallow slab and had low oxidizing capacity relative to fluids or melts which interacted with the mantle in the Izu-Bonin-Mariana arc and in the Cascades, which represent arc environments with comparable glass Fe XANES measurements. A simple framework accounts for local and global variability in fO_2 in fractionation-corrected glasses, where fluids of variable oxidizing capacity interact with depleted mantle to produce hydrous melts. The inheritance of volatile and fluid-mobile elements in regions of the mantle that undergo partial melting does not necessarily lead to higher fO_2 if the oxidizing capacity of the infiltrating hydrous fluids are melts is low. In back-arcs and near-trench environments, partial melts formed by interaction with fluids of low oxidizing capacity are similar to arc melts in their volatile contents, trace element, and isotopic signatures, but modestly oxidized relative to mid-ocean ridge basalts.

* Corresponding author.
E-mail addresses: Lee.Saper@jpl.nasa.gov (L.M. Saper), mbrounce@ucr.edu (M. Brounce), dominic.woelki@minpet.uni-freiburg.de (D. Woelki), r.cao-4@sms.ed.ac.uk (R. Cao), geoffrey.bromiley@ed.ac.uk (G. Bromiley).
[1] Present address: Jet Propulsion Laboratory, California Institute of Technology, Pasadena, CA, United States

https://doi.org/10.1016/j.epsl.2023.118560
Received 20 August 2023; Received in revised form 20 December 2023; Accepted 23 December 2023
Available online 9 January 2024

1. Introduction

The oxygen fugacity (fO_2) recorded by magmas varies systematically across tectonic settings (Carmichael et al., 1991; Cottrell et al., 2022), with an increase in fO_2 from basalts formed in mid-ocean-ridge environments (MORB), to those formed in back-arc basins (BABB), to relatively oxidized melts formed in arc environments. The increase in fO_2 across these tectonic settings is attributed to recycling of oxidized materials derived from subducting slabs into regions of the mantle that undergo partial melting (Wood et al., 1990; Ballhaus et al., 1991; Parkinson and Arculus, 1999; Kelley and Cottrell, 2009; Brounce et al., 2014; 2021; Birner et al., 2018; Muth and Wallace, 2021). However, the identity of the materials and processes that are responsible for the oxidation remains elusive (Evans and Tompkins, 2022). Oxidation in subduction zone environments has been attributed to addition of slab-derived sulfate (Muth and Wallace, 2021; Taracsák et al., 2023), dissociation of slab-derived H_2O (Tollan and Hermann, 2019), and aqueous slab-derived fluids or hydrous melts with high concentrations of dissolved oxidants (i.e., high oxidizing capacity; Kelley and Cottrell, 2009; Brounce et al., 2021). In this paper, we define "high" oxidizing capacity as a fluid with sufficient concentrations of oxidants such that interactions with mantle and melts increases the bulk Fe^{3+}/Fe^{2+} ratio and thus fO_2.

In subduction environments such as the Izu-Bonin-Mariana (IBM) system, increases in Fe^{3+}/Fe^{2+} ratios measured in glasses, which reflect higher fO_2 levels, correlate with elevated concentrations of dissolved volatiles and trace elements that track slab involvement, such as enrichments in large ion lithophile elements relative to rare earth elements (REE) (e.g., Ba/La and Rb/Sm, Brounce et al., 2014; 2021). However, in some locations including at the southern Mariana margin, fO_2 appears to be decoupled from volatile contents and proxies for slab influence (e.g., at the Fina Nagu volcanic chain, Brounce et al., 2016); such decoupling has also been documented by oxybarometry of variably metasomatized peridotites in the Canadian Cordillera (Kilgore et al., 2018). Therefore, the link between slab involvement and oxidation of the mantle source regions for subduction-related melts is complex, and assessing the relationship between fO_2 and melt chemistry in quenched glasses is critical for understanding the degree to which interactions with slab-derived fluids modify the fO_2 in melting environments influenced by subduction. The effect of slab fluids on fO_2 is important because volatile contents and fO_2 control phase equilibria and processes related to mantle melting (Carmichael and Ghiorso, 1990; Parkinson and Arculus, 1999; Bénard et al., 2018; Davis and Cottrell, 2021), melt transport and differentiation (Cottrell and Kelley, 2011; Brounce et al., 2014; Le Voyer et al., 2015; Birner et al., 2018; O'Neill et al., 2018; Brounce et al., 2021; Hu et al., 2023), and volatile cycling (Shorttle et al., 2015; Moussallam et al., 2016; Hartley et al., 2017; Brounce et al., 2017; 2021).

The Troodos Ophiolite is a well-preserved example of Late Cretaceous oceanic crust (Mukasa and Ludden, 1987). Compared to modern MORB, the Troodos mantle and its melts contain elevated H_2O and fluid-mobile trace element concentrations (e.g., Ba, Rb, Sr, U, and Pb), interpreted to be related to subduction processes (Rautenschlein et al., 1985; Pearce and Robinson, 2010). Due to its preservation and exposure, the Troodos Ophiolite has been crucial to our understanding of how oceanic crust is generated in the vicinity of convergent margins and represents an important target to evaluate the relationship between slab influence and fO_2 in subduction-influenced melting environments. However, the precise tectonic setting and the influence of subduction on melting and differentiation processes in the Troodos is debated (Flower and Levine, 1987; Pearce and Robinson, 2010; Regelous et al., 2014; Woelki et al., 2018; Hu et al., 2021; 2023; Ribeiro et al., 2023). All the interpretations of tectonic setting require interaction of subduction-derived materials with a highly depleted mantle to explain the high H_2O and fluid-mobile element concentrations measured in volcanic glasses, and the depletion in incompatible elements relative to MORB (e.g., Ti, Na, K, high-field-strength elements; Danyushevsky et al., 1993; Portnyagin et al., 1997; Coogan et al., 2003; Regelous et al., 2014; Woelki et al., 2019; Hu et al., 2021; Ribeiro et al., 2023). Radiogenic Pb and Sr isotopes (Rautenschlein et al., 1985; Woelki et al., 2018; Taylor et al., 2022) and stable B isotopes (Fonseca et al., 2017) measured in volcanic glasses suggest a role for sediment-derived fluids or melts in the petrogenesis of Troodos lavas, and such signatures are correlated spatially across the ophiolite (Woelki et al., 2018; Taylor et al., 2022). However, fO_2 has been quantified accurately in only one location at Troodos (at Marki using olivine-spinel oxybarometry; Hu et al., 2023) and given the geochemical complexity observed across the ophiolite it remains unclear whether variability in subduction-derived components correlates systematically with fO_2. Additionally, the timing and style of metasomatism of the Troodos melting region is less certain, for example whether the geochemistry and fO_2 are consistent with a subduction initiation setting (Pearce and Robinson, 2010; Hu et al., 2023) or a complex configuration such as a back-arc propagating into fore-arc crust (Regelous et al., 2014; Woelki et al., 2018; 2019; 2020).

In this study, we measured Fe and S speciation in quenched glasses collected from across the Troodos Ophiolite to quantify the variability in fO_2 recorded by the lavas, and to assess the degree to which slab-derived materials modified the fO_2 of the melting region and its derivative melts. We then compare the fO_2 and compositions of glasses from the Troodos Ophiolite with fO_2 estimates from glasses collected at mid-ocean ridge and subduction zone settings which have comparable measurements of Fe speciation and glass chemistry. Such comparisons reveal that the Troodos lavas share a close affinity with basalts formed in back-arc and near-trench settings and represent an endmember in which the inheritance of slab-derived volatiles and fluid-mobile elements by previously depleted mantle did not lead to significant oxidation.

2. Methods

2.1. Sample description

Volcanic glasses collected from across the extrusive section of the Troodos Ophiolite were characterized previously for their major and minor element, trace element, volatile and isotopic compositions (see Woelki et al., 2018; 2019; 2020 for a complete description of these samples). The glasses in this study represent 43 wafers analyzed for H_2O and CO_2 concentrations using Fourier-transform infrared spectroscopy (Woelki et al., 2020). The glasses are basaltic andesites and are classified either as boninitic (MgO >8 wt.%, TiO_2 <0.5 wt.%, SiO_2 >52 wt.%; Le Bas, 2000) or tholeiitic (following Woelki et al., 2018).

2.2. Fe and s micro X-ray absorption near-edge spectroscopy (XANES)

Fe and S XANES analyses were performed at beamline 13-IDE at the Advanced Photon Source (APS), Argonne National Laboratory. Fe XANES data acquisition and reduction were based on Cottrell et al. (2018) using the cryogenic Mössbauer calibration from Zhang et al. (2018); S XANES acquisition and reduction followed the techniques described by Brounce et al. (2021). Uncertainties reported for both Fe and S XANES correspond to the distribution of replicate measurements made on the same glass wafer and are reported as 1σ. Fe speciation was quantified in optically clear glass wafers; five altered samples (Woelki et al., 2020) were not optically clear. The altered glasses were measured using S XANES. Details on XANES analysis and data reduction, microphotographs of glass wafers, and corresponding XANES spectra can be found in the Supplement.

3. Results

3.1. Fe and S speciation in quenched glasses from the Troodos Ophiolite

The $Fe^{3+}/\sum Fe$ ($\sum Fe = Fe^{2+} + Fe^{3+}$) measured in the glass wafers

ranges from 0.125 to 0.156 (Table 1). The $Fe^{3+}/\sum Fe$ ratios increase with decreasing MgO contents (Fig. 1a), and thus vary with elements which are themselves correlated with MgO. There is no systematic relationship between Fe speciation and sampling location across the ophiolite (Fig. S1), however we note that the three glasses with the highest MgO contents and lowest $Fe^{3+}/\sum Fe$ ratios were collected from Kapilio at the southern margin. $Fe^{3+}/\sum Fe$ ratios do not correlate with trace element proxies for contribution of subduction-derived components such as Ba/La, Ce/Pb and S/Dy (Fig. 2a-c), nor are $Fe^{3+}/\sum Fe$ ratios correlated with dissolved volatile contents (H_2O, S and CO_2; Fig. S2) or with radiogenic Pb and Sr isotopes (Fig. S3). These relationships will be revisited in the following section where $Fe^{3+}/\sum Fe$ measurements are converted into calculations of fO_2.

In the unaltered glasses, $S^{6+}/\sum S$ ($\sum S = S^{2-} + S^{6+}$) ranges from 0.16 to 0.53 (Table 1) and are positively correlated with MgO (Fig. 1b) and with $Fe^{3+}/\sum Fe$ (Fig. 1c). $Fe^{3+}/\sum Fe$ and $S^{6+}/\sum S$ co-determined in glass wafers overlap within error of calculations of Fe-S redox equilibria in anhydrous silicate melts (black curve in Fig. 1c; O'Neill and Mavrogenes, 2022). Taken collectively, the speciation of Fe and S in unaltered volcanic glasses display an increase in the oxidized species with decreasing MgO contents. Importantly, they are not correlated with trace element proxies for slab involvement, nor with dissolved volatiles (Fig. S2) and radiogenic Pb and Sr isotopes (Fig. S3). The altered glasses (ellipse in Fig. 1b) all have systematically low $S^{6+}/\sum S$ (≤ 0.06); in 3 of the 5 altered glasses no S^{6+} peak was identified ($S^{6+}/\sum S \approx 0$). The altered glasses deviate from the trends defined by the relatively pristine glasses (Fig. 1b) and are not representative of magmatic values.

4. Discussion

4.1. Calculation of fO_2 from Fe and S XANES data of volcanic glasses from Troodos

The correspondence of Fe and S speciation measured in Troodos glasses with models of Fe-S redox equilibria (Fig. 1c) suggests the that glasses represent melts that were in redox equilibrium upon quenching

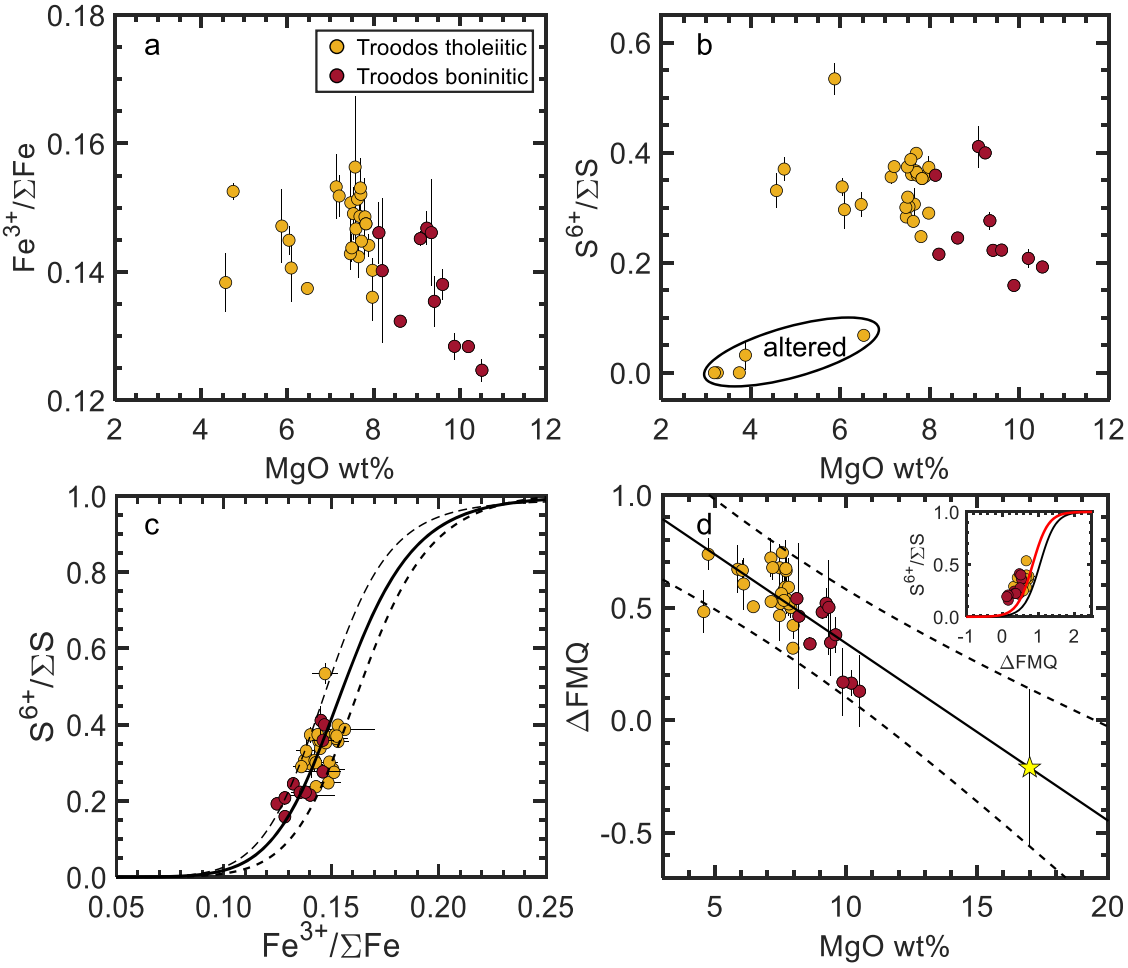

Fig. 1. Speciation of Fe and S measured using XANES in quenched volcanic glasses from the Troodos Ophiolite. Red circles are boninitic glasses and orange circles are tholeiitic glasses, as defined in Section 2.1. $Fe^{3+}/\sum Fe$ ratios were calculated following Cottrell et al. (2018) using the cryogenic Mössbauer calibration of Zhang et al. (2018); $S^{6+}/\sum S$ ratios were calculated using unscaled peak ratios following Brounce et al. (2021). Error bars are 1σ. **(a)** MgO wt.% vs. $Fe^{3+}/\sum Fe$, **(b)** MgO wt.% vs. $S^{6+}/\sum S$; the five glasses in the ellipse are altered (Woelki et al., 2020) and do not have corresponding Fe XANES measurements, **(c)** $Fe^{3+}/\sum Fe$ vs. $S^{6+}/\sum S$. The black curve was calculated using equation (13) in O'Neill and Mavrogenes (2022) evaluated at 1200 °C using the glass composition of CY16-glass-135 (Woelki et al., 2020); the dashed lines represent 1σ uncertainties. (d) MgO wt.% vs. fO_2 expressed as log unit deviations from the FMβQ buffer of Frost, 1991 (ΔFMQ), calculated as described in Section 4.1 using the Fe oxybarometer of Borisov et al. (2018). The solid line is a linear fit weighted by uncertainties in the Fe XANES measurements plus an additional 0.38 $\log_{10}$ unit standard error in the calculation of fO_2 from Fe^{3+}/Fe^{2+} (Borisov et al., 2018), resulting in Eq. (1): $1.129 \pm 0.459 - 0.079 \pm 0.058$[MgO *wt.*%]; $r^2 = 0.49$, MgO = 4.6 – 10.5 wt.%. The dashed lines are 95% prediction intervals. The yellow star represents the calculated fO_2 projected to the olivine liquidus at MgO = 17.5 wt.%: FMQ–0.21±0.35(2σ). The inset shows calculated ΔFMQ vs. $S^{6+}/\sum S$ in the Troodos glasses. The curves in the inset show two parameterizations of ΔFMQ vs. $S^{6+}/\sum S$; the red curve is the model of Jugo et al. (2010) for hydrous tholeiite recalculated to 1200 °C using the *T*-dependence of O'Neill and Mavrogenes (2022); the black curve was calculated following O'Neill and Mavrogenes (2022).

Table 1
Fe and S XANES measurements of unaltered glasses from the Troodos ophiolite (Woelki et al., 2018; 2019; 2020). Fe speciation was calculated following Cottrell et al. (2018); S speciation was calculated following Brounce et al. (2021) with no scaling factors. Quench T was calculated using Putirka (2008) eq. 15; fO_2 was calculated using Borisov et al. (2018) and is expressed in log units relative to the FMβQ buffer of Frost (1991).

Glass ID	Location	$Fe^{3+}/\sum Fe$	1σ	$S^{6+}/\sum S$	1σ	Quench T (°C)	ΔFMQ	1σ
CY1621	Limni	0.141	0.005	0.296	0.036	1112	0.605	0.115
CY1660	Pareklisia	0.145	0.001	0.411	0.038	1181	0.480	0.029
CY1661	Pareklisia	0.147	0.003	0.399	0.011	1187	0.519	0.066
CY1664	Pareklisia	0.144	0.002	0.357	0.010	1161	0.499	0.047
CY16-GLASS-12	Limni	0.137	0.000	0.306	0.023	1126	0.503	0.002
CY16-GLASS-129	Kapilio	0.132	0.001	0.245	0.003	1169	0.338	0.027
CY16-GLASS-135	Kapilio	0.125	0.002	0.192	0.008	1211	0.128	0.160
CY16-GLASS-144	Kapilio	0.128	0.001	0.208	0.018	1205	0.164	0.057
CY16-GLASS-150	Kapilio	0.128	0.002	0.159	0.011	1199	0.168	0.150
CY16-GLASS-184	Pareklisia	0.153	0.005	0.356	0.012	1139	0.720	0.085
CY16-GLASS-24	Limni	0.151	0.006	0.283	0.008	1148	0.676	0.103
CY16-GLASS-30	Limni	0.140	0.011	0.215	0.004	1165	0.461	0.322
CY16-GLASS-35	Limni	0.147	0.006	0.534	0.028	1110	0.670	0.106
CY16-GLASS-37	Limni	0.145	0.002	0.338	0.015	1119	0.665	0.045
CY16-GLASS-89	Pareklisia	0.146	0.008	0.276	0.016	1189	0.501	0.210
CY16-GLASS-95	Pareklisia	0.140	0.002	0.373	0.020	1163	0.420	0.058
CY16-PK-21	Pareklisia	0.135	0.004	0.222	0.001	1188	0.345	0.149
CY16-PK-7	Pareklisia	0.138	0.002	0.223	0.004	1189	0.379	0.078
CY17-AK7	Arakapas	0.142	0.003	0.306	0.029	1155	0.582	0.073
CY17-KV-104	Kalavassos	0.147	0.002	0.360	0.011	1154	0.567	0.051
CY17-KV-11	Kalavassos	0.146	0.005	0.359	0.000	1163	0.539	0.113
CY17-KV-113	Kalavassos	0.145	0.001	0.359	0.001	1153	0.538	0.012
CY17-KV-14	Kalavassos	0.149	0.003	0.367	0.019	1154	0.590	0.064
CY17-KV-39	Kalavassos	0.152	0.006	0.364	0.013	1153	0.663	0.106
CY17-KV-44	Kalavassos	0.152	0.003	0.375	0.002	1144	0.677	0.059
CY17-KV-48	Kalavassos	0.144	0.002	0.374		1148	0.518	0.053
CY17-KV-51	Kalavassos	0.153	0.002	0.399	0.000	1154	0.673	0.038
CY17-KV-53	Kalavassos			0.319		1155		
CY17-KV-56	Kalavassos	0.149	0.006	0.247	0.006	1155	0.590	0.127
CY17-KV-79	Kalavassos	0.156	0.014	0.387	0.003	1154	0.744	0.230
CY18-AR-13	Akaki	0.138	0.005	0.331	0.032	1082	0.482	0.127
CY18-AR-15	Akaki	0.153	0.001	0.370	0.021	1086	0.736	0.022
CY18-EA-16	Arakapas	0.136	0.004	0.290	0.010	1166	0.319	0.156
CY18-EA-31	Arakapas	0.149	0.004	0.302	0.000	1155	0.561	0.096
CY18-EA-36	Arakapas	0.143	0.002	0.300	0.005	1153	0.464	0.071
CY18-MA-7	Margi	0.147	0.000	0.353	0.010	1160	0.516	0.000
ET-6–2	Akaki	0.151	0.000	0.275	0.005	1162	0.532	0.000
CY17-KV-50	Kalavassos	0.143	0.004	0.237	0.007	1142	0.526	0.111

and permits calculating fO_2 of each glass at its quench temperature (T), which ranges from 1092 to 1218 °C (Table 1; eq. 15 in Putirka, 2008). Dissolved S^{6+} was detected in all the unaltered glasses (Fig. 1b); because the transitional fO_2 range over which S^{2-} converts to S^{6+} in natural silicate melts is narrow (e.g., Jugo et al., 2010; O'Neill and Mavrogenes, 2022; Boulliung and Wood, 2023), S speciation acts as a sensitive oxybarometer for these glasses and provides a test for whether fO_2 calculations, which are quantified using Fe speciation, produce internally consistent results. We calculated fO_2 using three Fe oxybarometers (Fig. S4) and concluded that the fO_2 values calculated using Borisov et al. (2018) were most successful in reconciling both the Fe and S speciation data from Troodos at a common T and fO_2, and so this model was adopted. The corresponding fO_2 of the Troodos glasses calculated at their quench T and expressed as log units relative to the fayalite--magnetite-β-quartz (FMQ) oxygen buffer (Frost, 1991) ranges from FMQ+0.13±0.16 to FMQ+0.74±0.23 (the ± value is propagated from 1σ XANES errors; Fig. 1d).

The fO_2 values account for the effects of T and melt composition on Fe^{3+}/Fe^{2+} ratios, and when fO_2 is used as the independent variable to compare to compositional variables, it produces trends that are more coherent than when using $Fe^{3+}/\sum Fe$ as the independent variable. For example, the increases in fO_2 with decreasing MgO (Fig. 1d) and S/Dy (Fig. 2f) are more clearly defined than the corresponding increases in $Fe^{3+}/\sum Fe$ (Fig. 1a; Fig. 2c). A linear least squares fit of MgO wt.% vs. ΔFMQ for the Troodos glasses, weighted by uncertainties in the Fe XANES measurements and in the fO_2 calculation (Borisov et al., 2018), produces the following equation (shown in Fig. 1d):

$$\Delta FMQ = 1.129 \pm 0.459 - 0.079 \pm 0.058 \times [MgO\ wt.\%] \quad (1)$$

Although the uncertainties are large, the slope in Eq. (1) overlaps with the MgO-fO_2 slope calculated for MORB with MgO = 5.5–10 wt.% (slope = –0.08±0.01; Cottrell and Kelley, 2011; O'Neill et al., 2018) and with the slope calculated for fore-arc basalts (FAB) from IBM (slope = –0.08, Brounce et al., 2014). Such correspondence in the amount of oxidation per decrement in MgO contents is important because the aforementioned MORB and FAB glasses have substantially lower H_2O contents (typically <1 wt.%,) compared to the Troodos glasses (2.2 ± 0.6 wt.% H_2O), suggesting that the MgO-fO_2 relationship is independent of H_2O contents at the level of precision with which we can currently quantify fO_2 based on Fe speciation (see Section 4.3.3) even though liquid lines of descent will depend on H_2O.

The relationship between MgO and fO_2 in the Troodos lavas is consistent with oxidation during closed-system crystallization of olivine with minor chromite (Hu et al., 2023) and indicates that the fO_2 of the Troodos volcanic suite was not externally buffered during differentiation, similar to conclusions drawn for MORB (Cottrell and Kelley, 2011; Le Voyer et al., 2015; O'Neill et al., 2018), BABB from the Mariana Trough (Brounce et al., 2014), and FAB and boninites from IBM (Brounce et al., 2021). Chromite inclusions are observed in olivines from Troodos with molar Mg/(Mg+Fe) (Mg#) from ~0.93 (Hu et al., 2021; 2023) to ~0.86 (Portnyagin et al., 1997; with one outlier Mg# = 0.83 olivine) indicating that crystallization of the two phases occurred over a wide T interval. Therefore, Eq. (1) can be used to estimate the fO_2 of liquids more primitive than those represented by quenched glasses,

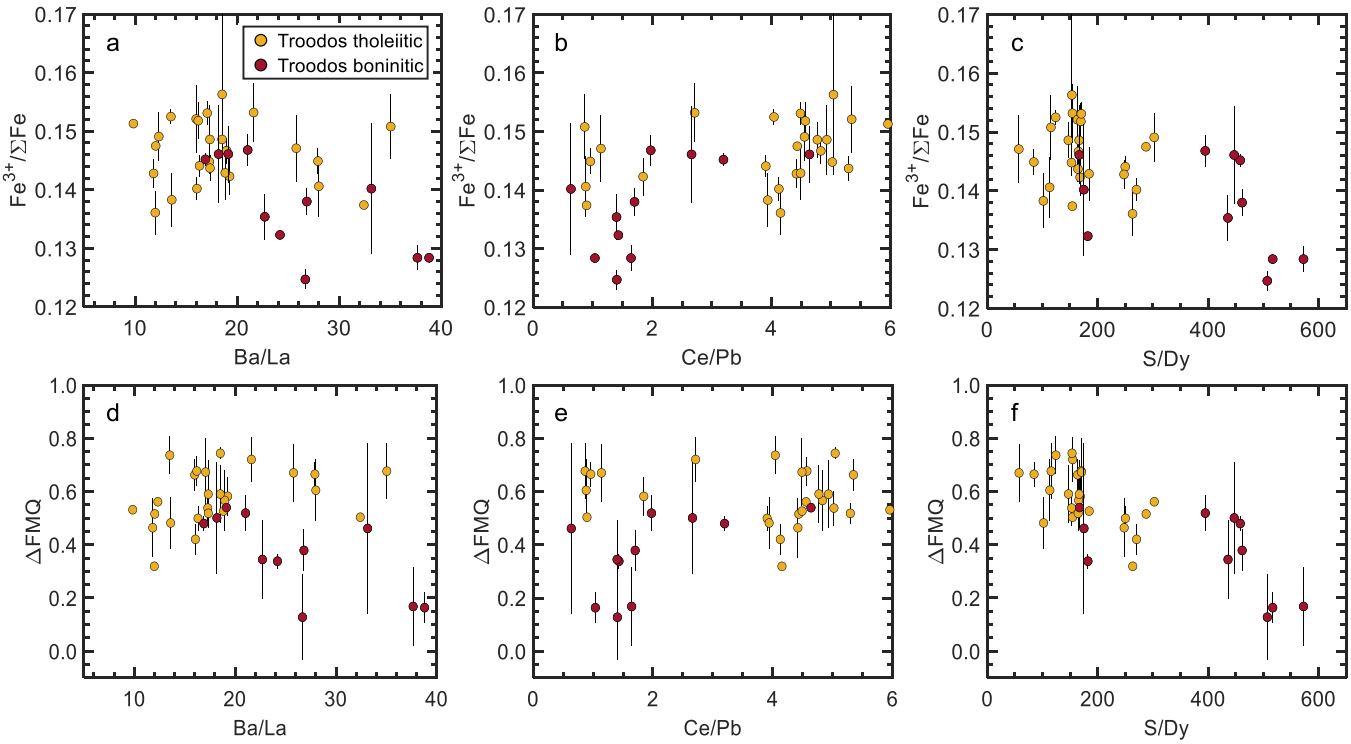

Fig. 2. Comparison of Fe XANES measurements of $Fe^{3+}/\sum Fe$ (top row) and fO_2 expressed as ΔFMQ (bottom row) in quenched glasses from the Troodos Ophiolite to trace element ratios that track subduction influence: Ba/La, **(a)** and **(d)**; Ce/Pb **(b)** and **(e)**, and S/Dy **(c)** and **(f)**. The fO_2 calculations are described in Section 4.1. Error bars are 1σ; ΔFMQ errors are propagated from the corresponding uncertainties in $Fe^{3+}/\sum Fe$ measurements. Trace element data are from Woelki et al. (2018; 2019; 2020) and are reproduced in the Supplementary Data.

which have a maximum MgO = 10.5 wt.%. At an fO_2 of ΔFMQ=0, melts in equilibrium with Mg# = 0.93 olivine have MgO contents of roughly 17.5 wt.% (Saper et al., 2022); projecting Eq. (1) to this MgO content, the fO_2 of the corresponding primitive olivine-saturated liquid at Troodos is FMQ–0.21±0.17 (yellow star in Fig. 1d).

Calculated fO_2 values are uncorrelated with Ba/La (Fig. 2d) and Ce/Pb (Fig. 2e), two trace element ratios which track the influence of slab fluids in the petrogenesis of Troodos lavas (Rautenschlein et al., 1985; Regelous et al., 2014; Woelki et al., 2019). Other commonly used trace element proxies for slab influence such as Ba/Ta, Th/Ta, Th/Nb (e.g., Pearce et al., 2005) are correlated with MgO in our glasses (Fig. S5). Trace element ratios in Troodos glasses involving severely depleted high-field-strength elements (e.g., Nb and Zr contents as low as 0.25 and 3.4 ppm) are dominated by variability in these elements rather than by enrichments in fluid-mobile elements, and so they are not reliable proxies for slab influence (Woelki et al., 2018; 2020). Complexities arising from previous episodes of melt depletion are addressed in Section 4.3.3. The glasses display a weak negative correlation between fO_2 and S/Dy (Fig. 2f) and total S contents (Fig. 3a), and fO_2 is uncorrelated with dissolved H_2O (Fig. 3b) and CO_2 (Fig. 3c). Radiogenic Pb and Sr isotopes demonstrate involvement of sediments and subduction fluids in the Troodos mantle source (Rautenschlein et al., 1985; Fonseca et al., 2017; Woelki et al., 2018; Taylor et al., 2022), however there is no correlation between fO_2 and these isotopic systems (Fig. 4).

The lack of correlation between fO_2 and H_2O (Fig. 3b), and between H_2O and S (Fig. S6), suggests that degassing was not a primary control on the variability in fO_2 of the lavas. The weak negative correlation of S and fO_2 (Fig. 3a) is opposite of the effect expected for degassing of melts with $S^{6+}/\sum S$ <0.5 (Hughes et al., 2023; Ding et al., 2023). Forward degassing models (Fig. S6; Ding et al., 2023) demonstrate that the range in glass S contents cannot be explained by a single degassing trend; plausible (though non-unique) degassing paths that can explain the H_2O

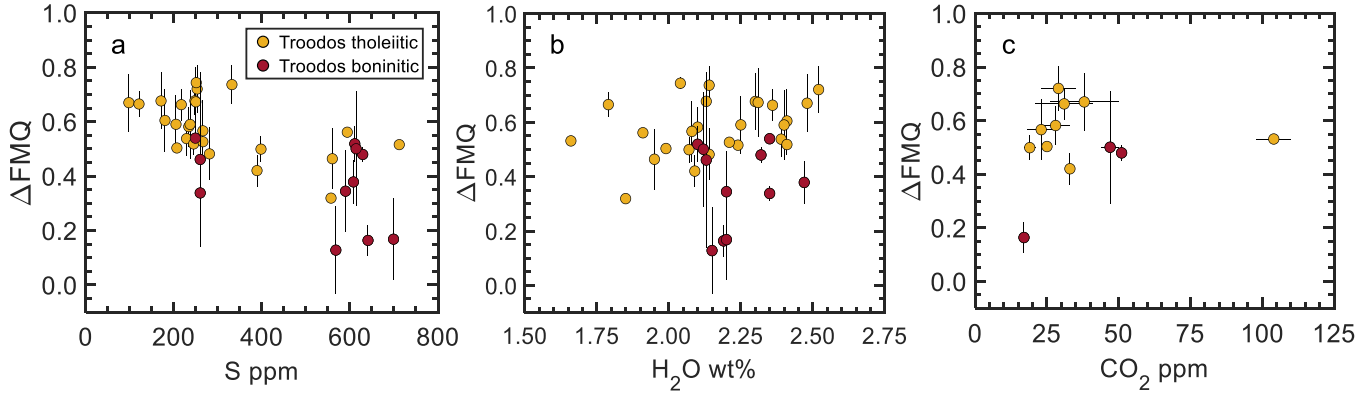

Fig. 3. Volatile contents versus calculated fO_2 expressed as ΔFMQ in Troodos Ophiolite glasses. **(a)** S (ppm), **(b)** H_2O (wt.%), **(c)** CO_2 (ppm). Volatile data are from Woelki et al. (2020).

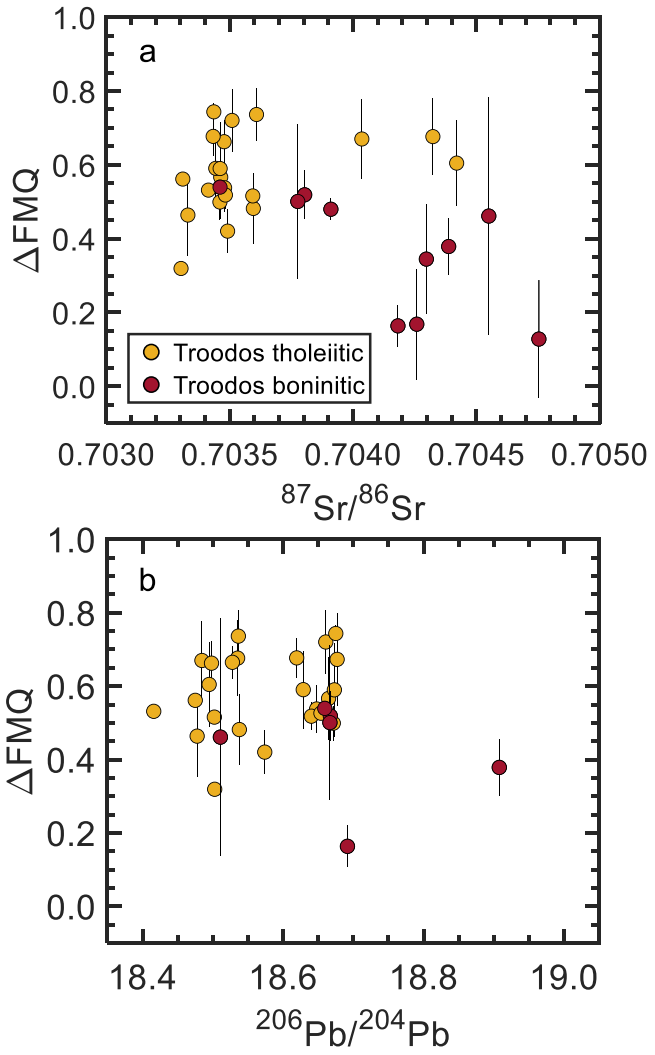

Fig. 4. Measurements of Sr and Pb isotopes in Troodos Ophiolite glasses versus calculated fO_2 expressed as ΔFMQ. **(a)** $^{87}Sr/^{86}Sr$, **(b)** $^{206}Pb/^{204}Pb$. Isotope data are from Woelki et al. (2020).

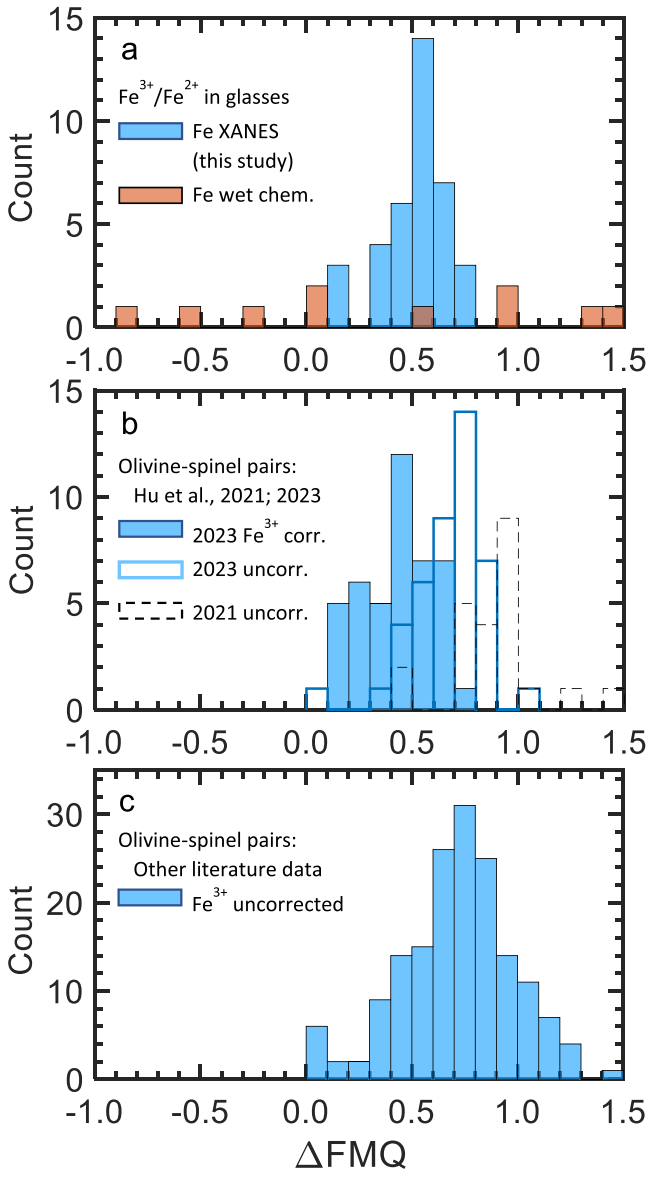

Fig. 5. Histograms comparing estimates of fO_2 of volcanic rocks from the Troodos Ophiolite calculated using different techniques and materials. **(a)** Fe oxybarometry of quenched glasses. The blue histogram shows fO_2 calculated from Fe XANES measurements of glasses from across the ophiolite (this study), the orange histogram represents fO_2 calculations from Fe^{3+}/Fe^{2+} ratios measured by wet chemistry in glasses from Akaki Canyon (Rautenschlein et al., 1985). **(b)** Olivine-spinel oxybarometry of chromian spinel inclusions in olivine in picritic pillow lavas from Marki (Hu et al., 2021; 2023). *T* is calculated using Li et al. (1995) with no correction for silica activity. The dashed black-outlined and unfilled blue-outlined histograms show calculations where Fe^{3+} in spinel was calculated based on charge balance (uncorrected, "uncorr.") using olivine-spinel data from Hu et al. (2021) and Hu et al. (2023), respectively. The filled blue histogram shows calculations where the Fe^{3+} value in spinel was corrected ("corr.") using Mössbauer-calibrated secondary standards (Davis et al., 2017; Hu et al., 2023). **(c)** Olivine-spinel oxybarometry from other locations in the Troodos Ophiolite, with Fe^{3+} calculated using charge balance (uncorrected). The data are from lower pillow lavas (Portnyagin et al., 1997) and upper pillow lavas (Sobolev et al., 1996; Golowin et al., 2017; Woelki et al., 2019). All olivine-spinel fO_2 calculations were done at 1000 bars, following Hu et al. (2023), and expressed as log units relative to the FMβQ buffer of Frost (1991).

vs. S relationships have fO_2 paths that are orthogonal to those shown in Fig. 3a. Degassing of CO_2 has a minor effect on fO_2 (Brounce et al., 2017; Ding et al., 2023). Thus, the fO_2 variability at Troodos is decoupled from its volatile contents, and degassing cannot explain the range in S contents dissolved in the glasses, nor the relationship between fO_2, H_2O and S. Calculated fO_2 values increase with increasing Cl, which is negatively correlated with MgO; Cl/K ratios rule out assimilation of Cl-rich crustal materials in Troodos lavas (Woelki et al., 2020), therefore the observed increase in fO_2 with decreasing MgO contents is not due to assimilation and is interpreted to result from crystal fractionation.

4.2. Comparison to previous estimates of the fO_2 of Troodos magmatic rocks

Wet chemistry determined $Fe^{3+}/\sum Fe$ ratios of glasses from Akaki Canyon vary from 0.08 to 0.20 (Rautenschlein et al., 1985), spanning a wider range than our Fe XANES measurements ($Fe^{3+}/\sum Fe$ = 0.125–0.156), which include three glasses from Akaki canyon ($Fe^{3+}/\sum Fe$ = 0.138–0.151). If the reported loss on ignition values (1.97–3.88 wt.%; Rautenschlein et al., 1985) are attributed to dissolved H_2O (in our unaltered glasses, H_2O ranges from 1.67 to 2.52 wt.%), the fO_2 corresponding to these wet chemical data can be calculated as described in Section 4.1. The range in calculated fO_2 is FMQ–0.88 to

FMQ+1.42 (Fig. 5a); the mean and standard deviation of the nine glasses is FMQ+0.25±0.76, which overlaps with the fO_2 values calculated from Fe XANES measurements in three Akaki Canyon glasses: FMQ+0.48, FMQ+0.53, FMQ+0.74 (Table 1).

The fO_2 calculated for cumulate gabbros from Troodos using Fe^{3+} partitioning between plagioclase and olivine ranges from FMQ+0.25 to FMQ+3.5 (median is FMQ+1.5), at an estimated *T* of 1045–1145 °C and pressure *(P)* = 1.5 kb (Coogan et al., 2003). Based on Fe*-Ti and Fe*-MgO systematics, Pearce & Robinson (2010) estimated that the Troodos complex formed approximately at FMQ+1. These estimates are high relative to the fO_2 values calculated from our glass Fe XANES measurements.

The remaining fO_2 estimates of volcanic rocks at Troodos are based on the Fe^{3+} contents of chromian spinels included in olivine phenocrysts in lavas. Considering only spinel data with Fe^{3+} contents adjusted using Mössbauer-calibrated secondary standards, olivine-spinel pairs in pillow lavas from Marki (Hu et al., 2023) have a distribution of fO_2 values at the olivine-spinel *T* (1123–1234 °C; Li et al., 1995) of FMQ+0.43±0.17 (Fig, 5b), which is in excellent agreement with the tholeiitic glass from Marki measured by XANES (FMQ+0.52 at a quench $T = 1160$ °C) and with the distribution of both boninitic and tholeiitic glasses from across the ophiolite (FMQ+0.52±0.15; $T = 1155\pm45$ °C; Fig. 5a). When projected to the olivine liquidus *T*, the olivine-spinel pairs provide an independent estimate of the primary melt fO_2 of FMQ–0.52±0.20 (Hu et al., 2023), which is lower than but overlaps within 1σ of the estimate based on projecting Eq. (1) to MgO = 17.5 wt.%, FMQ–0.21±0.17. These estimates both overlap within uncertainty of the fO_2 of olivine, spinel, and orthopyroxene bearing harzburgitic residues at Troodos, which when projected to 6 kb and 1355 °C have a calculated fO_2 of FMQ–0.58±0.46 (Hu et al., 2023).

Adjustment of Fe^{3+} values in spinels measured by microprobe using Mössbauer-calibrated secondary standards is critical for both the accuracy and precision of fO_2 values calculated from olivine+spinel ±orthopyroxene oxybarometry (Davis et al., 2017); the correction applied in Hu et al. (2023) results in ~20–25% lower $Fe^{3+}/\sum Fe$ ratios relative to uncorrected values calculated using charge balance (Fig. 5b). Hu et al. (2023) compared their fO_2 estimates using corrected spinel measurements to earlier studies with uncorrected spinel measurements and concluded that the olivines from Marki, some of which contain partially crystallized boninitic melt inclusions (Hu et al., 2021), were more reduced at their source conditions than olivines from tholeiitic lavas collected elsewhere in the ophiolite. To compare the olivine-spinel datasets in an internally consistent manner, we have calculated fO_2 at the olivine-spinel *T* (Li et al., 1995), using spinel Fe^{3+} values based on charge balance (i.e., uncorrected). The uncorrected olivine-spinel estimates of fO_2 at Marki (Hu et al., 2023) are indistinguishable at the 1σ level from olivine-spinel pairs in pillow lavas collected elsewhere in Troodos (compare the unfilled blue-outlined histogram in Fig. 5b to Fig. 5c). Thus, the interpretation that olivines at Marki crystallized from boninitic melts with distinctly lower fO_2 than olivines from elsewhere in the ophiolite (Hu et al., 2023) is biased by comparison of fO_2 estimates from corrected and uncorrected spinel Fe^{3+} contents. In contrast to this interpretation, the corrected olivine-spinel data from Marki overlap with our XANES data of glasses from Marki and from glasses collected across the ophiolite, which collectively show no difference in fO_2 based on glass type (e.g., boninitic vs. tholeiitic; Fig. 1d) nor by sampling location (Fig. S1).

The fO_2 values calculated from Fe-XANES measurements of volcanic glasses from the Troodos Ophiolite are consistent with derivation from primitive melts with indistinguishable initial fO_2 levels, and do not require variable fO_2 in time nor in space in the melting region. This may reflect a roughly uniform redox state in the Troodos mantle sources during melting, and/or from aggregation of fractional melts which homogenized larger-scale redox heterogeneities (Birner et al., 2018). Although there is compelling evidence for spatial variability in both the types and degrees of slab influence in Troodos lavas (Woelki et al., 2019; 2020; Taylor et al., 2022), our XANES results suggest that higher fluid inputs did not lead to commensurate increases in the fO_2 as a function of sampling location (Fig. S1). The average fO_2 of Troodos lavas was FMQ+0.52±0.15 upon quenching at the Cretaceous seafloor, representing a maximum increase in fO_2 of roughly one log unit between melt extraction and eruption.

4.3. Comparison to literature Fe XANES measurements in volcanic glasses from different tectonic settings

4.3.1. $Fe^{3+}/\sum Fe$ and calculated fO_2 values

Fe XANES data of glasses from MORB, fore-arc and back-arc spreading centers, and of glass inclusions from arc volcanoes are compared to Troodos in Fig. 6. Ocean island basalts were excluded due to low-*P* S degassing, which for melts with low H_2O/S leads to significant reduction of melt $Fe^{3+}/\sum Fe$ ratios (Shorttle et al., 2015; Hartley et al., 2017; Moussallam et al., 2016; Brounce et al., 2017). The effects of degassing on fO_2 are minimized in this compilation due to (1) high pressures of eruption of seafloor glasses, and (2) high H_2O/S ratios in arc melt inclusions compared to ocean island basalts (Brounce et al., 2017; 2021). The $Fe^{3+}/\sum Fe$ ratios measured in Troodos glasses overlap with MORB and IBM FAB at a given MgO content (Fig. 6a) and have lower $Fe^{3+}/\sum Fe$ than IBM boninites, arc volcanoes in Mariana, and Lassen Volcano in the Cascades (Fig. 6a).

For each glass, fO_2 was calculated as described in Section 4.1 (Borisov et al., 2018) using the reported glass composition and Fe^{3+}/Fe^{2+} ratio (Zhang et al., 2018). When accounting for the effects of *T* and melt composition (including the effect of H_2O on the liquidus *T*; Putirka, 2008), at a given $Fe^{3+}/\sum Fe$ ratio the Troodos glasses are more oxidized than MORB (Fig. 6b) and have an fO_2 distribution that overlaps with IBM FAB, Mariana trough BABB, and the near-trench volcanic chain of Fina Nagu at the southern Mariana margin (Brounce et al., 2014, 2016). As observed in Troodos (Fig. 1d), $Fe^{3+}/\sum Fe$ and fO_2 generally increase with decreasing MgO contents (Cottrell and Kelley, 2011; Brounce et al., 2014; O'Neill et al., 2018), which reflects crystallization of phases with lower $Fe^{3+}/\sum Fe$ than the coexisting liquids (Carmichael, 1991; Kelley and Cottrell, 2012; Brounce et al., 2014; O'Neill et al., 2018; Cottrell et al., 2022).

4.3.2. Volatile contents and trace element proxies for slab involvement

Dissolved volatile contents are linked to the redox state of silicate melts due to the efficacy with which degassing (particularly of S-bearing gasses) can modify fO_2 (Shorttle et al., 2015; Hartley et al., 2017; Moussallam et al., 2016; Brounce et al., 2017; 2021; Ding et al., 2023), and evidence that volatiles derived from subducted oceanic lithosphere drive changes in the oxidation state of the overlying mantle and its derivative melts (Kelley and Cottrell, 2009; Brounce et al., 2014; 2021; Muth and Wallace, 2021; 2022; Taracsák et al., 2023). For the depths at which the Troodos glasses were erupted (corresponding to vapor saturation *P* of ~400–500 bars; Woelki et al., 2020; Belgrano et al., 2021), and for the relatively undegassed arc melt inclusions in our compilation (Brounce et al., 2014; 2016; 2021; Muth and Wallace, 2021), the effects of degassing on fO_2 are expected to be minor (Fig. S6; Le Voyer et al., 2015; Moussallam et al., 2016; Brounce et al., 2017; Ding et al., 2023; Hughes et al., 2023). This is because effect of degassing on fO_2 is driven primarily by degassing of S at low *P* (<200–300 bars; Ding et al., 2023; Hughes et al., 2023), and forward degassing calculations suggest that such fO_2 changes in Troodos magmas were <0.2 $\log_{10}$ units (Fig. S6; Ding et al., 2023). The Troodos glasses and IBM boninites overlap in their H_2O contents, however the Troodos glasses are more reduced (Fig. 7a); conversely, although IBM FAB and Troodos overlap in their calculated fO_2 values, the Troodos glasses contain substantially more dissolved H_2O. Therefore, for the degree to which primitive melts in Troodos were enriched in H_2O, the lavas are systematically more reduced than comparably hydrous boninites from IBM and glass inclusions from the Mariana and Cascades arc (Fig. 7a).

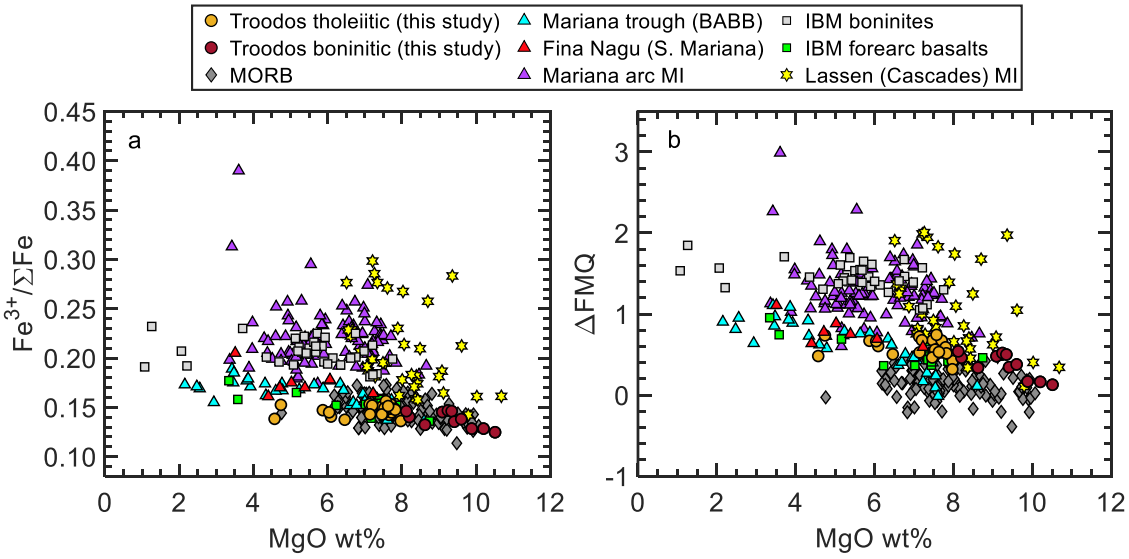

Fig. 6. Literature compilation of quenched glasses with Fe^{3+}/Fe^{2+} ratios determined by XANES. All Fe^{3+}/Fe^{2+} ratios were calculated following Cottrell et al. (2018) and Zhang et al. (2018); fO_2 was calculated using Borisov et al. (2018) at a quench T calculated from Putirka (2008) eq. 15, following the same approach described in Section 4.1 for the Troodos glasses. **(a)** MgO vs. $Fe^{3+}/\sum Fe$, **(b)** MgO vs. ΔFMQ. MI = melt inclusions; all other data are from matrix glasses. MORB: gray diamonds; Izu-Bonin-Mariana (IBM) boninites: gray squares; IBM fore-arc basalts, green squares; Mariana trough back-arc basalts: cyan triangles; Fina Nagu southern Mariana margin: red triangles; Mariana island-arc melt inclusions: purple triangles; Lassen volcano (Cascade arc) melt inclusions: yellow stars. Data sources: Troodos Ophiolite, this study; MORB, Kelley and Cottrell (2009); Cottrell and Kelley (2011; 2013); Le Voyer et al. (2015), Berry et al. (2018), Birner et al. (2018); Lerner et al. (2021); Mariana arc melt inclusions, Brounce et al. (2014); Fina Nagu, Brounce et al. (2016); IBM boninites and FAB, Brounce et al. (2021); Cascades arc, Lassen segment melt inclusions, Muth and Wallace (2021).

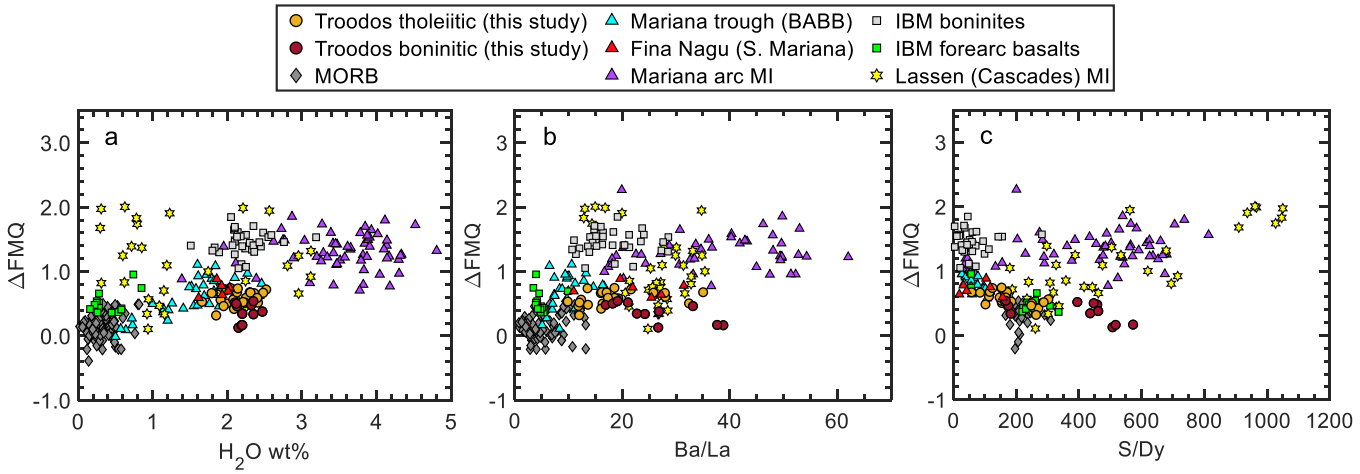

Fig. 7. ΔFMQ versus glass measurements of **(a)** H_2O wt.%, **(b)** Ba/La, and **(c)** S/Dy. The symbols and data sources are the same as in Fig. 6.

In addition to high dissolved volatile contents in the Troodos glasses, elevated values of fluid-mobile elements track interaction of slab-derived fluids with the Troodos mantle source (Rautenschlein et al., 1985; Pearce and Robinson, 2010; Regelous et al., 2014; Woelki et al., 2018; 2020). Positive correlations between fO_2 and trace element ratios that record slab-derived materials in arc glasses (Fig. 7b,c; Fig. S7) reflect oxidative metasomatism of the mantle by slab-derived fluids and/or melts (Brounce et al., 2014, 2021; Muth and Wallace, 2021; Tarascák et al., 2023). However, while the range in Ba/La in Troodos glasses (Ba/La = 8–56, Woelki et al., 2018; 2019) extends to substantially higher ratios compared to MORB (Ba/La <15) and overlaps with the elevated ratios measured in arc volcano glasses in our compilation (Ba/La = 13–62), the Troodos fO_2 values are uncorrelated with Ba/La (Fig. 2d), and for a given Ba/La they are more reduced than arc melt inclusion glasses (Fig. 7b). The same observation holds for other markers for slab influence (e.g., Cs/Th, Rb/Th, Sr/Nd; see Fig. S7).

The volatile contents and fO_2 of glasses from the Troodos share a close affinity with the fO_2 and composition of glasses from the Mariana trough (Brounce et al., 2014) and in particular with Fina Nagu at the southern Mariana margin (Brounce et al., 2016), overlapping not only in their major element compositions, fO_2 (Fig. 6b) and H_2O contents (Fig. 7a), but also with proxies for slab involvement (Fig. 7b,c; Fig. S7). In these locations, quenched melts have elevated quantities of fluid-mobile and volatile elements relative to MORB but with only modest increases in fO_2. The fluids or melts which infiltrated the melting regions in these locations were similarly low in their oxidizing capacities relative to the bulk Fe^{3+}/Fe^{2+} of the preexisting mantle.

In the central Mariana trough, samples which overlap with the fO_2 of MORB at similar MgO contents are dominated by decompression melting of upper mantle. There, the relatively large distance between the back-arc and trench, and a steeply dipping slab, leads to minor contributions of melt influenced by subduction (Stolper and Newman,

1994; Brounce et al., 2014). In the southern Mariana trough the subducting slab is 50–200 km depth directly below the back-arc spreading center and melting is dominated by fluxing of oxidized slab fluids into the melting column, manifested as quenched glasses with higher Fe^{3+}/Fe^{2+} ratios relative to the central trough (Brounce et al., 2014). At Fina Nagu in the far south, the slab is very shallow and directly below the volcanoes, corresponding to a change in the composition of slab-derived fluids delivered to the melting region (Brounce et al., 2016). Fina Nagu melts are dominated by flux melting, but by shallow slab fluids which had relatively low oxidizing capacity. At Fina Nagu, the resulting fO_2 levels of erupted melts are as reduced as those in the distal central Mariana trough, despite Fina Nagu capturing higher degrees of slab influence. Based on its similarities to Fina Nagu, the extensional melting environment which produced the Troodos extrusive series was likely dominated by dehydration of a shallow slab (Pearce and Robinson, 2010; Woelki et al., 2020; Belgrano et al., 2021; Ribeiro et al., 2023), producing relatively reduced fluids and minimal modification of the fO_2 of the overlying mantle and its derivative melts.

The S/Dy ratio tracks contributions of slab-derived S to the mantle source in arc settings; positive correlations with fO_2 and $\delta^{34}S$ have been interpreted as evidence that addition of slab-derived S^{6+} species drives oxidation in the subarc mantle (Muth and Wallace, 2021; 2022). In contrast to the positive relationship between fO_2 and S/Dy in the Cascades and the Marianas (Muth and Wallace, 2021; 2022; Fig. 7c), the Troodos glasses display a negative relationship between the two parameters — samples with the highest S/Dy are the most reduced. As with the compositional parameters described above, the fO_2 vs S/Dy trend defined by the Troodos glasses overlap with those from the Mariana trough and Fina Nagu, and also with IBM FAB and MORB (Fig. 7c). If the elevated S/Dy in the array of glasses that extends to lower fO_2 values is due to addition of slab-derived S to their respective mantle sources, then it suggests that the metasomatic fluids in these locations had low concentrations of S^{6+}. This is consistent with the fluids being low in their oxidizing potential compared to those in Mariana and Cascade arcs. The dissolved S^{6+} measured in the Troodos glasses results from oxidation due to closed-system crystallization (Fig. 1b,d); at the projected T-fO_2 conditions for melt extraction (yellow star in Fig. 1d; Hu et al., 2023) all S is calculated to have initially been dissolved as S^{2-} (O'Neill and Mavrogenes, 2022; Boulliung and Wood, 2023). The lack of correlation between fO_2 and fluid-mobile element proxies for slab involvement in a subset of subduction-influenced environments demonstrates that slab-derived fluids have variable oxidizing capacities, and that the fO_2 of the mantle proximal to subducting slabs can be decoupled from interaction with slab-derived fluids or melts.

4.3.3. *A framework to explain metasomatism, melting, and fO_2 in subduction-influenced environments*

Melting processes influence trace element properties of mantle melts and can potentially affect fO_2; for example, it is debated whether melting leads to progressive reduction (Bénard et al., 2018), to slight oxidation (Bézos et al., 2005), or to little or no change in fO_2 (O'Neill et al., 2018; Birner et al., 2021; Davis and Cottrell, 2021). Here, we outline a framework that can simultaneously account for the effects of melting, volatile contents and fO_2, in the context of our compilation of glasses from ocean ridges and subduction-influenced environments. Glasses with MgO ≥5.5 wt.% were corrected for low-P fractionation to a common MgO content of 8 wt.%, accounting for the effects of H_2O on liquid lines of descent (e.g., Ti_8 is wt.% TiO_2 projected to MgO = 8 wt.%; Langmuir et al., 2006; Bézos et al., 2009). Following the observation that the slope of MgO vs. ΔFMQ is roughly constant for each tectonic setting in our compilation (Fig. 6b; Fig. S8), fO_2 values were corrected for fractionation using a uniform slope ($\delta[\Delta FMQ]/\delta[MgO\ wt.\%] = -0.08$) to produce the parameter $[\Delta FMQ]_8$; this is used instead of $[Fe_2O_3]_8$ (Bézos and Humler, 2005; Davis and Cottrell, 2021) because there is sufficient compositional range in our compilation such that the activities of FeO and Fe_2O_3 in the melt are influenced by composition (Borisov et al., 2018) and cannot be compared directly to infer differences in fO_2 (e.g., compare Fig. 6a to Fig. 6b). The systematics do not change if instead we used the calculated fO_2 values shown in Fig. 6b, or by using MgO vs. ΔFMQ relationships fit individually to each suite of glasses (e.g., Fig. S8), or by empirically reconstructing the major and minor element chemistry of the glasses to MgO = 8 wt.% (including Si_8, Al_8, $[Fe_2O_3]_8$, $[FeO]_8$, etc.) and recalculating fO_2 at the wet liquidus T (Fig. S9).

The Ti_8 of MORB decreases with increasing average melt fraction (F) (Langmuir et al., 2006). At constant T, addition of H_2O increases F, and the effect diminishes with increasing H_2O such that in plots of Ti_8 vs. H_8 hydrous melting curves are concave up and become increasingly steep with increasing F and decreasing Ti_8 (Fig. 8a; Langmuir et al., 2006). In contrast, straight negatively sloped lines in this space represent mixing of a dry MORB-like component with hydrous subduction-influenced melts; this construction explains the variation in Ti_8 vs. H_8 observed in back-arcs such as the Mariana trough (Langmuir et al., 2006). In addition to increasing F, increasing H_2O is linked to higher fO_2 in arc environments (Kelley and Cottrell, 2009; Cottrell et al., 2022). Therefore, in plots of Ti_8 vs. $[\Delta FMQ]_8$ (Fig. 8b) oxidative flux melting, or mixing of reduced dry melts and oxidized hydrous melts, leads to negatively sloped curves that intersect the low-H_8 MORB array (dashed lines in Fig. 8b). The magnitude of the slope of the intersecting line reflects the oxidizing capacity of the hydrous fluid, and the intersection with the MORB array reflects the degree of depletion in the unmetasomatized mantle source. Note that the slope of Ti_8 vs. $[\Delta FMQ]_8$ for MORB is indistinguishable from zero.

The geochemically similar hydrous glasses from the Troodos Ophiolite, Mariana trough, and Fina Nagu lie above the MORB array in Fig. 8b. The Troodos glasses represent a depleted endmember with low Ti_8 due to high degrees of melt extraction (Arculus and Parkinson, 1999; Regelous et al., 2014) and with elevated H_8 contents overlapping with IBM boninites (Fig. 8a). The hydrous fluids that infiltrated the mantle source of the Troodos lavas must have been less oxidizing compared to the fluids involved in generating IBM boninites, which have higher fO_2 despite overlapping H_8 and Ti_8 values. Note that a few glasses from Troodos with $Ti_8 > 0.5$ suggest limited mixing of hydrous melt with relatively dry and reduced melts similar to MORB, consistent with inferences based on trace element and radiogenic isotope systematics (Woelki et al., 2019; Taylor et al., 2022).

Clockwise rotation from the MORB array reflects higher oxidizing capacity of slab-derived fluids. Flux melting with fluids of variable oxidizing capacity can account for redox variability within individual arcs (i.e., rotation around a particular intersection with the MORB array) and variable fO_2 at a given Ti_8 in different subduction zones. The geometric construction can explain why arcs have higher variance in fO_2 compared to extensional environments (Cottrell et al., 2022), which are dominated by mixing of melts derived from dry and wet, but both relatively reduced, mantle sources (Fig. 8a; Langmuir et al., 2006). For example, at Mariana both the increase in fO_2 from Agrigan volcano (sediment melt signature) to Guguan volcano (hydrous fluid signature) and the variability observed within Sarigan volcano (heterogeneous fluid-melt signature) (Kelley and Cottrell, 2012; Brounce et al., 2014) can be explained by sweeping upwards towards higher negative slopes in Ti_8 vs. $[\Delta FMQ]_8$ space, as the oxidizing capacity and influence of the slab-derived fluid increases. At Lassen Volcano, individual cinder cones (BORG, BPPC, BRM, and BBL) variably sample involvement of slab-derived fluids (Muth and Wallace, 2021). Cones derived from the cool portion of the slab beneath Lassen (BORG and BPPC; green stars in Fig. 8) represent hydrous flux melting by fluids of similar oxidizing capacity as in Mariana, whereas cones derived from a hotter slab (BRM and BBL; red and blue stars, respectively in Fig. 8), rise from the MORB array at a steeper angle and intersect the MORB array at higher Ti_8 values. The fO_2 variability within individual volcanoes at both Mariana and Lassen suggest that melt inclusions recovered from a single arc volcano may sample melts of heterogeneously oxidized mantle.

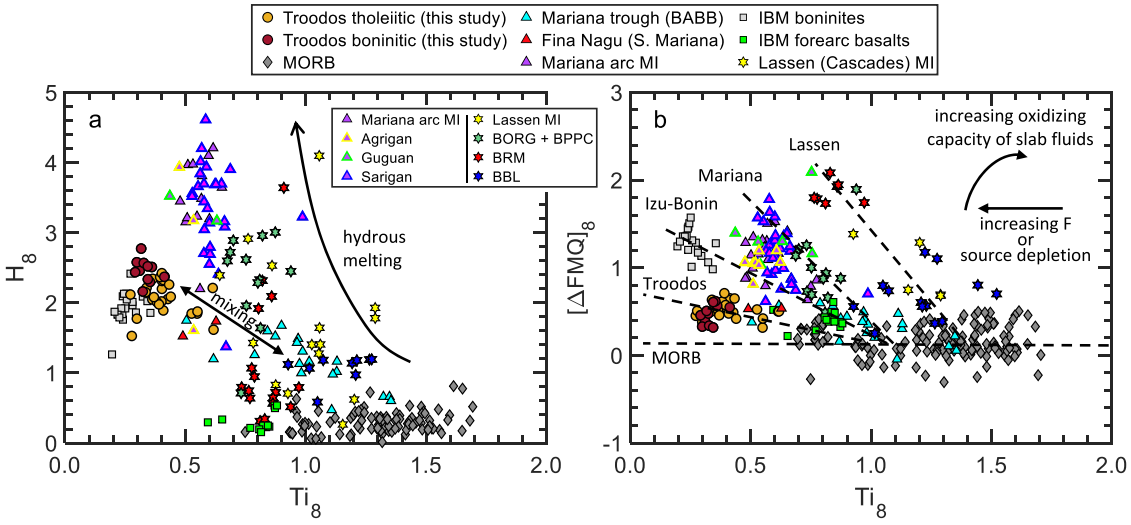

Fig. 8. **(a)** Ti_8 (wt.% TiO_2 corrected for low-*P* fractionation to MgO = 8 wt.%; Klein and Langmuir, 1987; Langmuir et al., 2006; Bézos et al., 2009) vs. H_8 (wt.% H_2O, fractionation corrected to MgO = 8 wt.%). Negatively sloped lines represent mixing trends between dry MORB-like melts and wet arc-like melts; concave up curves represent hydrous flux melting paths. **(b)** Ti_8 vs $[\Delta FMQ]_8$, where $[\Delta FMQ]_8$ is calculated by projecting fO_2 values calculated from glass Fe^{3+}/Fe^{2+} ratios and quench *Ts* (e.g., Fig. 6b) to MgO = 8 wt.% using a constant slope of $\delta[\Delta FMQ]/\delta[MgO\ wt.\%] = -0.08$ (see Section 4.3.3 and Figs. S8 and S9); this corrects for the modest oxidation that accompanies closed-system crystallization and allows for comparison of fO_2 between glasses representing a range of compositions and quench *Ts* (which vary at MgO = 8 wt.% due to variable H_2O contents and melt compositions). Lower values of Ti_8 correspond to higher average degrees of melting (*F*) or of source depletion. The labeled dashed lines qualitatively connect glasses from similar geographic locations and subduction zones. Increases in the magnitudes of the dashed-line slopes are interpreted to reflect increasing oxidizing capacities of metasomatic fluids; the intersection with the MORB field reflects the degree of melting or depletion of the mantle sources. The different colored symbols from the Mariana arc (triangles) and from Lassen (stars) represent melt inclusion data from individual volcanoes. The remaining symbols and data sources are the same as in Fig. 6.

For the Troodos Ophiolite, the fO_2 inferred from measurements of Fe^{3+}/Fe^{2+} ratios in quenched lavas do not require a multi-stage evolution in which the mantle was first reduced due to melting and then oxidized due to interaction with slab-derived fluids (e.g., during subduction initiation, Hu et al., 2023). Instead, they fit coherently within global systematics of subduction-influenced extensional melting environments (Fig. 8), where mantle melts sample a mixture of dry and damp sides of a melting prism (Langmuir et al., 2006; Bézos et al., 2009), and in which the infiltrating slab-derived fluids were dilute in oxidants compared to fluids involved in typical arc petrogenesis. If slab-derived S was delivered to the Troodos melting region (accounting for some of the range in S/Dy), then it is unlikely that metasomatism was dominated by oxidizing S^{6+}-bearing fluids (Hu et al., 2023). This is consistent with the source of fluids in Troodos being derived from a relatively shallow slab (Brounce et al., 2016; Woelki et al., 2020; Ribeiro et al., 2023), and possibly buffered by interaction with reduced sediment melts (Padrón-Navarta et al., 2023), which have been inferred to play a role in Troodos petrogenesis from measurements of glass B isotopes (Fonseca et al., 2017) and Pb isotopes (Rautenschlein et al., 1985; Woelki et al., 2018; Taylor et al., 2022). Such a scenario suggests that the inheritance of volatile and fluid-mobile elements in the mantle adjacent to subducting slabs can be largely decoupled from changes in fO_2 if the slab fluid does not contain the sufficient oxidative capacity, producing hydrous melts that are only slightly more oxidized than MORB. The conjugate arc front volcanoes represent hydrous flux melting by slab-derived fluids with variable oxidative capacities, but which are typically higher than those sampled in extensional environments.

5. Conclusion

1. Fe and S XANES measurements in glasses sampled from across the Troodos Ophiolite ($Fe^{3+}/\sum Fe = 0.125$–0.156; $S^{6+}/\sum S = 0.16$–0.53) indicate that the glasses preserve the redox state of melts at their quench *Ts* (1092–1218 °C), and represent a range in fO_2 of FMQ+0.13±0.16 to FMQ+0.74±0.23. Calculated fO_2 values increase with decreasing MgO contents and are uncorrelated with H_2O, trace element proxies for slab involvement, and radiogenic Pb and Sr isotopes. The lavas were derived from primary melts of indistinguishable initial fO_2 levels of approximately FMQ–0.21±0.17.
2. $Fe^{3+}/\sum Fe$ ratios in Troodos glasses overlap with MORB, however when accounting for the effects of *T*, melt composition, and crystal fractionation the Troodos lavas ($[\Delta FMQ]_8 = 0.50\pm0.11$) are slightly more oxidized than MORB ($[\Delta FMQ]_8 = 0.15\pm0.18$). Despite overlapping volatile contents, trace element proxies for slab involvement, and degrees of depletion from prior melting events, Troodos lavas and are more reduced than melt inclusions from IBM boninites and from arc volcanoes (average $[\Delta FMQ]_8 > 1.0$). The compositions, fO_2 range, and volatile contents of Troodos lavas share close affinities with Mariana trough back-arc basalts, the near-trench volcanoes of Fina Nagu at the southern Mariana margin, and with forearc basalts from IBM, which together display elevated volatile and fluid-mobile element contents with only modest increases in fO_2 relative to MORB.
3. The Ti_8 vs. $[\Delta FMQ]_8$ framework accounts for global fO_2 systematics of quenched melts as a function of the degree of depletion in their mantle sources and the oxidizing capacity of metasomatic fluids. As observed in the Troodos Ophiolite, the production of hydrous and fluid-mobile element enriched partial melts in extensional and near-trench environments can occur without significant oxidation due to interactions with fluids of low oxidizing capacity. Arc volcanoes represent hydrous flux melting influenced by slab-derived fluids or melts with variable but typically high oxidizing capacities.

Appendix A. Supplementary Materials

Supplementary materials describing XANES analysis and reduction techniques, optical images of glass wafers, and Fe and S XANES spectra can be accessed in the online version of this article.

CRediT authorship contribution statement

L.M. Saper: Writing – original draft, Visualization, Investigation,

Funding acquisition, Conceptualization. **M. Brounce:** Writing – review & editing, Validation, Investigation, Conceptualization. **D. Woelki:** Writing – review & editing, Resources. **R. Cao:** Formal analysis. **G. Bromiley:** Writing – review & editing, Supervision.

Declaration of competing interest

The authors declare that they have no known competing financial interests or personal relationships that could have appeared to influence the work reported in this paper.

Data availability

Supplementary Data, including glass compositions and raw Fe and S XANES spectra are provided in the Supplementary Tables.

Acknowledgements

We thank three anonymous reviewers and handling editor Laurence Coogan for their constructive feedback on this manuscript. This research used resources of the Advanced Photon Source, a U.S. Department of Energy (DOE) Office of Science User Facility operated for the DOE Office of Science by Argonne National Laboratory under Contract No. DE-AC02–06CH11357. We acknowledge the support of GeoSoilEnviroCARS (Sector 13), which is supported by the National Science Foundation - Earth Sciences (EAR-1634415).

Supplementary materials

Supplementary material associated with this article can be found, in the online version, at doi:10.1016/j.epsl.2023.118560.

References

Ballhaus, C., Berry, R.F., Green, D.H., 1991. High pressure experimental calibration of the olivine-orthopyroxene-spinel oxygen geobarometer: implications for the oxidation state of the upper mantle. Contrib. Mineral. Petrol. 107, 27–40.
Belgrano, T.M., Tollan, P.M., Marxer, F., Diamond, L.W., 2021. Paleobathymetry of submarine lavas in the Samail and Troodos Ophiolites: Insights from volatiles in glasses and implications for hydrothermal systems. J. Geophys. Res. Solid Earth 126 e2021JB021966.
Bénard, A., Woodland, A.B., Arculus, R.J., Nebel, O., McAlpine, S.R.B., 2018. Variation in sub-arc mantle oxygen fugacity during partial melting recorded in refractory peridotite xenoliths from the West Bismarck Arc. Chem. Geo. 486, 16–30.
Berry, A.J., Stewart, G.A., O'Neill, H.St.C., Mallmann, G., Mosselmans, J.F.W, 2018. A re-assessment of the oxidation state of iron in MORB glasses. Earth Planet. Sci. Lett. 483, 114–123.
Bézos, A., Escrig, S., Langmuir, C.H., Michael, P.J., Asimow, P.D., 2009. Origins of chemical diversity of back-arc basin basalts: A segment-scale study of the Eastern Lau Spreading Center. J. Geophys. Res. Solid Earth 14.
Bézos, A., Humler, E., 2005. The $Fe^{3+}/\sum Fe$ ratios of MORB glasses and their implications for mantle melting. Geochim. Cosmochim. Acta 69, 711–725.
Birner, S.K., Cottrell, E., Warren, J.M., Kelley, K.A., Davis, F.A., 2021. Melt addition to mid-ocean ridge peridotites increases spinel Cr# with no significant effect on recorded oxygen fugacity. Earth Planet. Sci. Lett. 566, 116951.
Birner, S.K., Cottrell, E., Warren, J.M., Kelley, K.A., Davis, F.A., 2018. Peridotites and basalts reveal broad congruence between two independent records of mantle fO_2 despite local redox heterogeneity. Earth Planet. Sci. Lett. 494, 172–189.
Borisov, A., Behrens, H., Holtz, F., 2018. Ferric/ferrous ratio in silicate melts: a new model for 1 atm data with special emphasis on the effects of melt composition. Contrib. Mineral. Petrol. 173, 98.
Boulliung, J., Wood, B.J., 2023. Sulfur oxidation state and solubility in silicate melts. Contrib. Mineral. Petrol. 178, 56.
Brounce, M.N., Kelley, K.A., Cottrell, E., 2014. Variations in $Fe^{3+}/\sum Fe$ of Mariana arc basalts and mantle wedge fO_2. J. Petrol. 55, 2513–2536.
Brounce, M., Kelley, K.A., Stern, R., Martinez, F., Cottrell, E., 2016. The Fina Nagu volcanic complex: Unusual submarine arc volcanism in the rapidly deforming southern Mariana margin. Geochem. Geosys. Geosyst. 17, 4078–4091.
Brounce, M., Stolper, E., Eiler, J., 2017. Redox variations in Mauna Kea lavas, the oxygen fugacity of the Hawaiian plume, and the role of volcanic gases in Earth's oxygenation. Proc. Nat. Acad. Sci 114, 8997–9002.
Brounce, M., Reagan, M.K., Kelley, K.A., Cottrell, E., Shimizu, K., Almeev, R., 2021. Covariation of slab tracers, volatiles, and oxidation during subduction initiation. Geochem. Geosys. Geosyst. 22, e2021GC009823.
Carmichael, I.S.E., Ghiorso, M.S., 1990. The effect of oxygen fugacity on the redox state of natural liquids and their crystallizing phases. Rev. Mineral. Geochem. 24, 191–212.
Carmichael, I.S.E., 1991. The redox states of basic and silicic magmas: a reflection of their source regions? Contrib. Mineral. Petrol. 106, 129–141.
Coogan, L., Banks, G., Gillis, K., MacLeod, C., Pearce, J., 2003. Hidden melting signatures recorded in the Troodos ophiolite plutonic suite: evidence for widespread generation of depleted melts and intra-crustal melt aggregation. Contrib. Mineral. Petrol. 144, 484–506.
Cottrell, E., Kelley, K.A., 2011. The oxidation state of Fe in MORB glasses and the oxygen fugacity of the upper mantle. Earth Planet. Sci. Lett. 305, 270–282.
Cottrell, E., Kelley, K.A., 2013. Redox heterogeneity in mid-ocean ridge basalts as a function of mantle source. Science 340, 1314–1317.
Cottrell, E., Lanzirotti, A., Mysen, B., Birner, S., Kelley, K.A., Botcharnikov, R., Davis, F. A., Newville, M., 2018. A Mössbauer-based XANES calibration for hydrous basalt glasses reveals radiation-induced oxidation of Fe. Am. Mineral. 103, 489–501.
Cottrell, E., Birner, S.K., Brounce, M., Davis, F.A., Waters, L.E., Kelley, K.A., 2022. Oxygen fugacity across tectonic settings. Magma Redox Geochemistry. American Geophysical Union (AGU), pp. 33–61.
Danyushevsky, L.V., Falloon, T.J., Sobolev, A.V., Crawford, A.J., Carroll, M., Price, R.C., 1993. The H_2O content of basalt glasses from Southwest Pacific back-arc basins. Earth Planet. Sci. Lett. 117, 347–362.
Davis, F.A., Cottrell, E., Birner, S.K., Warren, J.M., Lopez, O.G., 2017. Revisiting the electron microprobe method of spinel-olivine-orthopyroxene oxybarometry applied to spinel peridotites. Am. Mineral. 102, 421–435.
Davis, F.A., Cottrell, E., 2021. Partitioning of Fe_2O_3 in peridotite partial melting experiments over a range of oxygen fugacities elucidates ferric iron systematics in mid-ocean ridge basalts and ferric iron content of the upper mantle. Contrib. Mineral. Petrol. 176, 67.
Ding, S., Plank, T., Wallace, P.J., Rasmussen, D.J., 2023. Sulfur_X: A model of sulfur degassing during magma ascent. Geochem. Geosys. Geosyst. 24, e2022GC010552.
Evans, K.A., Tomkins, A.G., 2022. Redox variables and mechanisms in subduction magmatism and volcanism. Magma Redox Geochemistry. American Geophysical Union (AGU), pp. 63–91.
Flower, M.F.J., Levine, H.M., 1987. Petrogenesis of a tholeiite-boninite sequence from Ayios Mamas, Troodos ophiolite: evidence for splitting of a volcanic arc? Contrib. Mineral. Petrol. 97, 509–524.
Fonseca, R.O.C., Kirchenbaur, M., Ballhaus, C., Münker, C., Zirner, A., Gerdes, A., Heuser, A., Botcharnikov, R., Lenting, C., 2017. Fingerprinting fluid sources in Troodos ophiolite complex orbicular glasses using high spatial resolution isotope and trace element geochemistry. Geochim. Cosmochim. Acta 200, 145–166.
Frost, B.R., 1991. Introduction to oxygen fugacity and its petrologic importance. In: Lindsley, D.H. (Ed.), Oxide Minerals. De Gruyter, pp. 1–10.
Golowin, R., Portnyagin, M., Hoernle, K., Sobolev, A., Kuzmin, D., Werner, R., 2017. The role and conditions of second-stage mantle melting in the generation of low-Ti tholeiites and boninites: the case of the Manihiki Plateau and the Troodos ophiolite. Contrib. Mineral. Petrol. 172, 104.
Hartley, M.E., Shorttle, O., Maclennan, J., Moussallam, Y., Edmonds, M., 2017. Olivine-hosted melt inclusions as an archive of redox heterogeneity in magmatic systems. Earth Planet. Sci. Lett. 479, 192–205.
Hu, W.J., Zhou, M.F., Malpas, J., Ren, Z.Y, 2021. High-Ca boninitic melt inclusions in lavas of the Troodos ophiolite and a reappraisal of genetic relationships between different lava types. GSA Bull. 133, 1831–1850.
Hu, W.J., Zhou, M.F., Ribeiro, J.M., Malpas, J., Wu, Y.D., Bai, Z.J., 2023. The redox state of incipient oceanic subduction zones: An example from the Troodos Ophiolite (Cyprus). J. Geophys. Res. Solid Earth 128, e2022JB025008.
Hughes, E.C., Saper, L.M., Liggins, P., O'Neill, H.St.C., Stolper, E.M, 2023. The sulfur solubility minimum and maximum in silicate melt. J. Geol. Soc. (Lond.) 180, jgs2021–jgs2125.
Jugo, P.J., Wilke, M., Botcharnikov, R.E., 2010. Sulfur K-edge XANES analysis of natural and synthetic basaltic glasses: Implications for S speciation and S content as function of oxygen fugacity. Geochim. Cosmochim. Acta 74, 5926–5938.
Kelley, K.A., Cottrell, E., 2009. Water and the Oxidation State of Subduction Zone Magmas. Science 325, 605–607.
Kelley, K.A., Cottrell, E., 2012. The influence of magmatic differentiation on the oxidation state of Fe in a basaltic arc magma. Earth Planet. Sci. Lett. 329–330, 109–121.
Kilgore, M.L., Peslier, A.H., Brandon, A.D., Lamb, W.M., 2018. Water and oxygen fugacity in the lithospheric mantle wedge beneath the Northern Canadian Cordillera (Alligator Lake). Geochem. Geosys. Geosyst. 19, 3844–3869.
Klein, E.M., Langmuir, C.H., 1987. Global correlations of ocean ridge basalt chemistry with axial depth and crustal thickness. J. Geophys. Res. Solid Earth 92, 8089–8115.
Langmuir, C.H., Bézos, A., Escrig, S., Parman, S.W., 2006. Chemical systematics and hydrous melting of the mantle in back-arc basins. In: Christie, D.M., Fisher, C.R., Lee, S.M., Givens, S. (Eds.), Geophysical Monograph Series. American Geophysical Union, Washington, D. C, pp. 87–146.
Le Bas, M.J, 2000. IUGS Reclassification of the high-Mg and picritic volcanic rocks. J. Petrol. 41, 1467–1470.
Le Voyer, M., Cottrell, E., Kelley, K.A., Brounce, M., Hauri, E.H, 2015. The effect of primary versus secondary processes on the volatile content of MORB glasses: An example from the equatorial mid-Atlantic Ridge (5°N–3°S). J. Geophys. Res. Solid Earth 120, 125–144.
Lerner, A.H., Muth, M.J., Wallace, P.J., Lanzirotti, A., Newville, M., Gaetani, G.A., Chowdhury, P., Dasgupta, R., 2021. Improving the reliability of Fe- and S-XANES measurements in silicate glasses: Correcting beam damage and identifying Fe-oxide nanolites in hydrous and anhydrous melt inclusions. Chem. Geo. 586, 120610.

Li, J., Kornprobst, J., Vielzeuf, D., Fabriès, J., 1995. An improved experimental calibration of the olivine-spinel geothermometer. Chin. J. Geochem. 14, 68–77.
Moussallam, Y., Edmonds, M., Scaillet, B., Peters, N., Gennaro, E., Sides, I., Oppenheimer, C., 2016. The impact of degassing on the oxidation state of basaltic magmas: A case study of Kīlauea volcano. Earth Planet. Sci. Lett. 450, 317–325.
Mukasa, S.B., Ludden, J.N., 1987. Uranium-lead isotopic ages of plagiogranites from the Troodos ophiolite, Cyprus, and their tectonic significance. Geology 15, 825–828.
Muth, M.J., Wallace, P.J., 2021. Slab-derived sulfate generates oxidized basaltic magmas in the southern Cascade arc (California, USA). Geology 49, 1177–1181.
Muth, M.J., Wallace, P.J., 2022. Sulfur recycling in subduction zones and the oxygen fugacity of mafic arc magmas. Earth Planet. Sci. Lett. 599, 117836.
O'Neill, H.St.C., Berry, A.J., Mallmann, G, 2018. The oxidation state of iron in mid-ocean ridge basaltic (MORB) glasses: Implications for their petrogenesis and oxygen fugacities. Earth Planet. Sci. Lett. 504, 152–162.
O'Neill, H.St.C., Mavrogenes, J.A, 2022. The sulfate capacities of silicate melts. Geochim. Cosmochim. Acta 334, 368–382.
Padrón-Navarta, J.A., López Sánchez-Vizcaíno, V., Menzel, M.D., Gómez-Pugnaire, M.T., Garrido, C.J, 2023. Mantle wedge oxidation from deserpentinization modulated by sediment-derived fluids. Nat. Geosci. 16, 268–275.
Parkinson, I.J., Arculus, R.J., 1999. The redox state of subduction zones: insights from arc-peridotites. Chem. Geo. 160, 409–423.
Pearce, J.A., Stern, R.J., Bloomer, S.H., Fryer, P., 2005. Geochemical mapping of the Mariana arc-basin system: Implications for the nature and distribution of subduction components. Geochem. Geosys. Geosyst 6.
Pearce, J.A., Robinson, P.T., 2010. The Troodos ophiolitic complex probably formed in a subduction initiation, slab edge setting. Gond. Res. 18, 60–81.
Portnyagin, M.V., Danyushevsky, L.V., Kamenetsky, V.S., 1997. Coexistence of two distinct mantle sources during formation of ophiolites: a case study of primitive pillow-lavas from the lowest part of the volcanic section of the Troodos Ophiolite, Cyprus. Contrib. Mineral. Petrol. 128, 287–301.
Putirka, K.D., 2008. Thermometers and Barometers for Volcanic Systems. Rev. Mineral. Geochem. 69, 61–120.
Rautenschlein, M., Jenner, G.A., Hertogen, J., Hofmann, A.W., Kerrich, R., Schmincke, H. U., White, W.M., 1985. Isotopic and trace element composition of volcanic glasses from the Akaki Canyon, Cyprus: implications for the origin of the Troodos ophiolite. Earth Planet. Sci. Lett. 75, 369–383.
Regelous, M., Haase, K.M., Freund, S., Keith, M., Weinzierl, C.G., Beier, C., Brandl, P.A., Endres, T., Schmidt, H., 2014. Formation of the Troodos Ophiolite at a triple junction: Evidence from trace elements in volcanic glass. Chem. Geo. 386, 66–79.
Ribeiro, J., MacLeod, C.J., Lissenberg, C.J., 2023. Did the Troodos ophiolite of Cyprus form during subduction inception? Chem. Geo. 641, 121774.
Saper, L.M., Baker, M.B., Stolper, E.M., 2022. Fe^{2+}–Mg partitioning between olivine and liquid at low oxygen fugacity: an experimental and thermodynamic framework. Contrib. Mineral. Petrol. 177, 94.
Sobolev, A., Migdisov, A.A., Portnyagin, M., 1996. Incompatible element partitioning between clinopyroxene and basalt liquid revealed by the study of melt inclusions in minerals from Troodos lavas, Cyprus. Petrol 4, 307–317.
Shorttle, O., Moussallam, Y., Hartley, M.E., Maclennan, J., Edmonds, M., Murton, B.J., 2015. Fe-XANES analyses of Reykjanes Ridge basalts: Implications for oceanic crust's role in the solid Earth oxygen cycle. Earth Planet. Sci. Lett. 427, 272–285.
Stolper, E., Newman, S., 1994. The role of water in the petrogenesis of Mariana trough magmas. Earth Planet. Sci. Lett. 121, 293–325.
Taracsák, Z., Mather, T.A., Ding, S., Plank, T., Brounce, M., Pyle, D.M., Aiuppa, A., Eimf, 2023. Sulfur from the subducted slab dominates the sulfur budget of the mantle wedge under volcanic arcs. Earth Planet. Sci. Lett. 602, 117948.
Taylor, R.N., Ishizuka, O., Hessey, I., Michalik, A., Stillwell, L., White, S., 2022. Isotopes track Tethyan seamount subduction beneath the Troodos spreading centre, Cyprus. Earth Planet. Sci. Lett. 584, 117509.
Tollan, P., Hermann, J., 2019. Arc magmas oxidized by water dissociation and hydrogen incorporation in orthopyroxene. Nat. Geosci. 12, 667–671.
Woelki, D., Regelous, M., Haase, K.M., Romer, R.H.W., Beier, C., 2018. Petrogenesis of boninitic lavas from the Troodos Ophiolite, and comparison with Izu–Bonin–Mariana fore-arc crust. Earth Planet. Sci. Lett. 498, 203–214.
Woelki, D., Regelous, M., Haase, K.M., Beier, C., 2019. Geochemical mapping of a paleo-subduction zone beneath the Troodos Ophiolite. Chem. Geo. 523, 1–8.
Woelki, D., Michael, P., Regelous, M., Haase, K., 2020. Enrichment of H_2O and fluid-soluble trace elements in the Troodos Ophiolite: Evidence for a near-trench origin. Lithos 356–357, 105299.
Wood, B.J., Bryndzia, L.T., Johnson, K.E., 1990. Mantle oxidation state and its relationship to tectonic environment and fluid speciation. Science 248, 337–345.
Zhang, H.L., Cottrell, E., Solheid, P.A., Kelley, K.A., Hirschmann, M.M., 2018. Determination of $Fe^{3+}/\sum Fe$ of XANES basaltic glass standards by Mössbauer spectroscopy and its application to the oxidation state of iron in MORB. Chem. Geo. 479, 166–175.